METRICA
METRology Institutional CAtalog

ISTITUTO NAZIONALE DI RICERCA METROLOGICA
Repository Istituzionale

Magnetite-epoxy nanocomposites obtained by the reactive suspension method:
Microstructural, thermo-mechanical and magnetic properties

(Article begins on next page)

28 December 2024

Accepted Manuscript

Magnetite-epoxy nanocomposites obtained by the reactive suspension method: microstructural, thermo-mechanical and magnetic properties

G. Barrera, C. Sciancalepore, M. Messori, P. Allia, P. Tiberto, F. Bondioli

Please cite this article as: Barrera, G., Sciancalepore, C., Messori, M., Allia, P., Tiberto, P., Bondioli, F., Magnetite-epoxy nanocomposites obtained by the reactive suspension method: microstructural, thermo-mechanical and magnetic properties, *European Polymer Journal* (2017), doi: http://dx.doi.org/10.1016/j.eurpolymj.2017.07.022

Magnetite-epoxy nanocomposites obtained by the reactive suspension method: microstructural, thermo-mechanical and magnetic properties

G. Barrera,[a] C. Sciancalepore,[b] M. Messori,[c] P. Allia[*],[d] P. Tiberto[a] and F. Bondioli[b,e]

[a] I.N.Ri.M., Nanoscience and Materials, Strada delle Cacce 91, 10135, Torino, Italy.

[b] INSTM, Research Unit of Parma, Department of Industrial Engineering, University of Parma, Parco Area delle Scienze 181/A, 43124, Parma, Italy.

[c] Department of Engineering "Enzo Ferrari", University of Modena and Reggio Emilia, Via Vivarelli 10, 41125, Modena, Italy.

[d] Department of Applied Science and Technology, Polytechnic of Torino, Corso Duca degli Abruzzi 24, 10129, Torino, Italy.

[e] Department of Industrial Engineering, University of Parma, Parco Area delle Scienze 181/A, 43124, Parma, Italy.

*corresponding author. E-mail address: paolo.allia@polito.it (P. Allia).

Abstract

Magnetite nanoparticles are prepared by non-hydrolytic sol-gel process in the presence of iron(III)-acetylacetonate as precursor and 2-ethyl-1,3-hexanediol as reactive solvent; the nanoparticle size is affected by the precursor-to-solvent ratio. The suspensions, mixed with bisphenol-A diglycidyl ether, are cured in the presence of ytterbium(III) trifluoromethanesulfonate as cationic initiator. The chain-growth polymerization results in a three-dimensional network where the diol, acting at the same time as reactive solvent and suspending medium, is covalently linked to the epoxy network according to the "activated monomer" mechanism. The filler induces stiffening because of hydrodynamic effects and of a better cross-linking ability in the nanocomposite. Magnetite nanoparticles form aggregates whose size and shape depend on concentration. Isothermal magnetization loops and FC/ZFC DC susceptibility curves indicate that all nanocomposites are dominated by interparticle magnetic interactions resulting in a collective response whose details depend on nanoparticle concentration and degree of aggregation.

Keywords: magnetite nanoparticles; reactive suspension method; functional polymer nanocomposites; magnetic interactions

1. Introduction

Polymer nanocomposites, consisting of inorganic nanoparticles embedded in a polymeric matrix generally combine the properties of both organic and inorganic precursors. Incorporating inorganic nanoparticles into organic matrices allows one to get suitably modified polymeric materials with better thermo-mechanical properties and novel physical functionalities which can be tuned by varying composition, size and concentration of the

nanoparticulate inorganic fraction, leading to the design of materials specifically tailored to meet the needs of different end users [1,2].

Magnetic nanocomposites have attracted wide interest for their potential applications such as energy storage devices [3], electronic components [4], microwave absorbers [5] and sensors [6]. The properties of these composite materials can change with dispersion, shape, surface properties, mean size and size distribution of nanoparticles. Important advances in the knowledge of nanostructures have been achieved by studying nanomaterials whose magnetic response can be properly controlled (often in combination with other physical properties) by varying the amount and degree of aggregation of magnetic nanoparticles in the polymeric matrix [7]. Moreover, nanoparticle dispersions in polymers are exploited to address fundamental issues such as the role and effect of interparticle interactions in nanogranular systems: size, concentration, dispersibility and degree of aggregation of magnetic nanoparticles give rise to a variety of magnetic phases, ranging from almost pure superparamagnetic [8] to highly correlated [9].

In order to disperse inorganic fillers in a polymeric matrix, two general methods are usually followed: (i) *in situ* synthesis of nanoparticles in the polymer matrix [10] or *in situ* polymerization of an organic monomer in the presence of inorganic nanoparticles [11]; or (ii) incorporation of *ex situ* synthesized nanoparticles in organic polymers with the use of melts or solution mixing methods [12,13]. Between the two main synthetic routes, *in situ* nanoparticle preparation seems to be more advantageous because it allows to optimize the interaction between the polymeric matrix and the nanoparticle surface, avoiding the problems related to the incorporation of preformed nanofiller by means of mechanical mixing. In this framework, the sol-gel method is the most widely used technique. As a matter of fact, the sol–gel process has some advantages such as the use of metallo-organic precursors, organic solvents, low processing temperatures, processing versatility of the colloidal state, which collectively give rise to milder synthesis conditions and make the mixing between inorganic and organic components easier at the nanometer scale [14].

The so-called non-hydrolytic sol–gel (NHSG) process was recently proposed as an alternative to the traditional aqueous route commonly exploited to obtain a great variety of pure and crystalline metal oxides [15]. The flexibility of this synthetic approach is very important because it entails a chemical environment as much as possible compatible with the features of the polymer matrix [16,17]. Indeed in the NHSG reaction, the solvent not only reacts with the organometallic precursor but also it acts as a surface ligand, allowing

2

nanoparticle growth and nanoparticle surface functionalization to be controlled without the need of any additional reagents in the solution [18].

Recently, starting from NHSG reaction, an innovative *in situ* polymerization technique was developed for *one step* nanocomposite synthesis, adding the monomeric precursor and the cationic initiator solution directly in the reaction mixture of the nanoparticles, without any further preparation: in this way the nanofiller distribution and dispersion are optimized in the polymeric three-dimensional network [19,20]. The excess solvent, unreacted in the NHSG nanoparticle suspension, acts not only as a suspending medium for nanoparticles but also as reagent acting on organic monomers in the subsequent polymerization reaction. This double role of the solvent is the basis of the "reactive suspension method", used by the authors to prepare metal oxide nanoparticle filled polymers [21,22].

In this work, magnetite nanocomposites in epoxy matrix were obtained by this method using, for the first time to the authors' knowledge, 2-ethyl-1,3-hexanediol as reactive solvent for NHSG synthesis of magnetic nanoparticles, as capping agent and finally as reactive suspending medium. In fact, the alcoholic solvent was covalently linked to the epoxy network according to the activated monomer (AM) mechanism during the propagation step in the chain growth polymerization [23].

Magnetite nanoparticles and nanocomposites were structurally and morphologically characterized by TEM, XRD and FTIR; mechanical effects induced in the nanocomposites by the presence of magnetic nanoparticles were studied by dynamic and thermo-mechanical analysis. Magnetic properties of the as-prepared nanocomposites were measured at different temperatures between 5 and 300 K; the results were interpreted on the basis of the information stemming from microscopic, spectroscopic and structural analysis. In this way, a comprehensive picture of the states of aggregation among dissolved nanoparticles and of the effect of temperature on the stability of magnetic interparticle correlations has been achieved.

2. Experimental

2.1 Materials

Bisphenol A diglycidyl ether (DGEBA, Dow D.E.R.™ 332 with an epoxide equivalent weight of 172-176), 2-ethyl-1,3-hexanediol (HD), propylencarbonate (PC), ytterbium(III) trifluoromethanesulfonate hydrate (Yb(OTf)$_3$), and ethanol (EtOH) were purchased by

Sigma Aldrich (Milan, Italy). Acetylacetone (AcAcH) and iron(III) chloride hexahydrate ($FeCl_3 \cdot 6H_2O$) for the synthesis of iron(III) acetylacetonate were purchased from Carlo Erba (Milan, Italy). All materials were high purity reactants and were exploited without further purification.

2.2 Preparation of epoxy-magnetite nanocomposites

Different amounts of iron(III)-acetylacetonate ($Fe(AcAc)_3$) synthesized as reported by Bondioli et al. [9], were dissolved in 3g of HD in a 100 mL Schlenk tube in order to correlate the powder properties with a different precursor-to-solvent ratio (varying in the range $0.04 - 0.27$ (mol/mol); composition details are given in Table 1). Additional information on the synthesis procedure is given by Sciancalepore et al. [23] After reaction, the stable alcoholic suspensions were added to the epoxy resin (Table 1) to obtain composites with different amounts of Fe_3O_4 (ranging between 1 and 6 phr) with the aim of assessing the role of nanomagnetite on the structural and functional properties of nanocomposites. A typical thermally-curable formulation was obtained by mechanical mixing of magnetite suspension, DGEBA epoxy monomer and the solution of $Yb(OTf)_3$ in PC (1:3 wt/wt ratio) as thermal cationic initiator. The formulations were degassed by dynamic vacuum treatment to avoid bubble formation in the final specimens, and were subsequently cast into silicone molds (having cavity dimensions of $80 \times 10 \times 3$ mm^3). All samples were reacted at 120°C for 180 min and post-cured for 30 min at 150°C. The materials were coded as DGEBA-HD_x where x represents the nominal amount of magnetite expressed as phr and calculated from stoichiometry by assuming full conversion of $Fe(AcAc)_3$ to Fe_3O_4.

Composite Code	DGEBA	Yb(Otf)$_3$	HD	Fe(AcAc)$_3$	Nominal Fe$_3$O$_4$
	(g)	(g)	(g)	(g)	(phr)
DGEBA-HD_0	7	0.12	3	0.00	0
DGEBA-HD_1	7	0.12	3	0.32	1
DGEBA-HD_2	7	0.12	3	0.65	2
DGEBA-HD_4	7	0.12	3	1.29	4
DGEBA-HD_6	7	0.12	3	1.94	6

Table 1 Composition of the thermally-curable composite formulations

4

2.3 Characterization of magnetic nanopowders

Particles morphology and grain-size distribution were examined by transmission electron microscopy (TEM; instrument: JEM 2010, Jeol, Japan). A drop from each suspension was put on a copper grid, covered with PELCO® support films of Formvar, and dried. Particles size analysis was performed on the obtained TEM images with the SPIP (Scanning Probe Imaging Processor, Image Metrology A/S, Denmark) software.

In order to better characterize the inorganic phase all powders were washed, put in a centrifuge until a colorless liquid phase was obtained, and finally dried under low pressure.

To identify the crystalline phase, the dried powders were analyzed by the Bragg-Brentano θ-2θ diffractometer X'Pert PRO (PANalytical, Netherlands), equipped with a graphite monochromator. The radiation source was an X-ray tube with copper radiation ($\lambda CuK_{\alpha1}, K_{\alpha2}$ = 1.540598, 1.544426 Å) and the anode tube load was 40 kV and 40 mA. Room-temperature X-ray diffraction (XRD) patterns were obtained in the 10-100° 2θ range, with a scanning rate of $0.0025° \cdot s^{-1}$ and a step size of $0.02°$ 2θ in the continuous scanning mode. Sample phase composition was confirmed by Raman spectroscopy. Raman-scattering experiments were carried out using a micro-Raman system (Labram instrument Jobin Yvon-Horiba) at room temperature. The 632.81 nm line of He-Ne laser was used for excitation with the exposure time of 60 s.

The qualitative characterization of the residual organic groups bound to the particle surfaces was done by means of Fourier transform infrared spectroscopy (FTIR) analysis on the obtained powders. The analysis was performed in the range 4000-500 cm^{-1}, using the Avatar 330 spectrometer (Thermo Nicolet, Germany), equipped with a diamond crystal, in the Attenuated Total Reflectance (ATR) mode.

2.4 Characterization of epoxy-magnetite nanocomposites

FT-IR spectroscopy was performed using an Avatar 330 FT-IR Thermo Nicolet spectrometer, equipped with a diamond crystal, operating in the ATR mode from 4000 to 500 cm^{-1} (64 scans and resolution of 1 cm^{-1}). Epoxy groups conversion values (α) were determined based on the signal at 910 cm^{-1}, corresponding to the asymmetric stretching of oxirane groups, normalized with respect to the signal at 1500 cm^{-1}, corresponding to C-C stretching of the aromatic ring. The parameter α was calculated through the equation:

$$\alpha = 100 - \left(\frac{A_{pc}}{A_{bc}} \cdot 100 \right) \tag{1}$$

5

where A_{bc} and A_{pc} are the normalized area of the signal at 910 cm^{-1} of the mixture before and after the curing, respectively.

Extraction tests were done by immerging the specimens (about 3 g each), wrapped in a fine net, into 50 ml of chloroform for 24 h at room temperature, according to an adaptation of the ASTM D2765 technical standard. The samples were subsequently dried to a constant mass (i.e., the dried mass m_d), and the absolute extractable fraction (f) was determined by the following equation (2):

$$f = \frac{m_0 - m_d}{m_0} \cdot 100 \tag{2}$$

where m_0 is the mass of the sample before its immersion in chloroform.

Scanning transmission electron microscopy (STEM) was carried out on nanocomposite samples to evaluate the distribution and dispersion of magnetite nanoparticles into epoxy resin and correlate the structural characteristics with the magnetic properties of nanocomposites. STEM images were obtained using the field emission gun-scanning electron microscopy (FEG-SEM) Nova NanoSEM 450 (FEI Company, USA) equipped with a STEM detector in the bright-field mode at primary beam energy of 30 keV. Initially the nanocomposite samples were trimmed into the shape of trapezoidal flat pyramids with a glass blade and then sectioned into ultrathin slices (70-100 nm) using a ultramicrotome REICHERT-JUNG Ultracut E (Reichert-Jung, Austria) equipped with a diamond knife (Micro Star Technologies, USA) and placed on Formvar-coated copper grids.

Differential scanning calorimetry (DSC) was done using a TA2010 (TA Instruments, New Castel, UK) at a scanning rate of 3°C·min^{-1} from 0 to 200°C under nitrogen flow. The glass transition temperature (T_g^{DSC}) was assumed coincident with the mean value of the energy jump of the thermogram (average value between the onset and the endpoint of the glass transition range).

Dynamic-mechanical thermal analysis (DMTA) was performed on rectangular strips (average length: 70 mm; average cross-section: 20 mm^2) by means of a TA Q800 (TA Instruments, New Castle, DE, USA) in the dual-cantilever configuration under a heating rate of 3°C·min^{-1}. The samples were examined under a displacement amplitude of 5 µm and a preload of 0.01 N at the oscillation frequency of 1 Hz. Storage modulus, E', and loss factor, $tan\ \delta$, were measured from -10°C up to the temperature at which the rubbery state was attained. Glass transition temperature, T_g^{DMTA}, was assumed at the maximum of the loss factor curves.

In order to compare the experimental results with data predicted by the Kerner's model for composite materials, the generalized Kerner's equation (3), as proposed by Nielsen [24], was used in the form:

6

$$\frac{E'}{E'_1} = \frac{1 + AB\phi_2}{1 - B\psi\phi_2} \tag{3}$$

E' and E'_1 being the storage moduli of composite and unfilled epoxy, respectively.

The constant A contains information on factors such as geometry of the filler phase and Poisson's ratio of the matrix. In the case of spherical filler particles and for any Poisson's ratio v, the constant A is defined as:

$$A = \frac{7 - 5v}{8 - 10v} \tag{4}$$

The constant B depends on the ratio between filler (E_2), and matrix (E_1) moduli and can be approximated to unity for very large moduli ratios.

The parameter ψ depends on the maximum packing fraction of the particles (ϕ_m) according to the following definition:

$$\psi = 1 + \frac{1 - \phi_m}{\phi_m^2}\phi_2 \tag{5}$$

where ϕ_2 is the filler volume fraction.

In this work the Poisson's ratio v of the matrix and the maximum packing fraction of the particles ϕ_m were taken respectively equal to 0.5 (epoxy in the rubbery state) and to 0.601 (random loose packing, not agglomerated packing configuration) [25].

Isothermal hysteresis loops were measured using a Quantum Design MPMS SQUID magnetometer (maximum field: 70 kOe) operating in the range 2 – 300 K. Field Cooled (FC) and Zero Field Cooled (ZFC) magnetization curves were measured between 10 and 300 K using a Lakeshore 7400 VSM magnetometer (maximum field: 17 kOe) equipped with a continuous-low cryostat, under an applied field of 200 Oe at a constant dT/dt rate of about 6 K/min.

3. Results and discussion

3.1 Fe_3O_4 powders characterization

XRD spectra (Fig. 1(a)) show that magnetite powders, independent of the precursor-to-solvent ratio, are characterized by the presence of a crystalline phase, identified as magnetite (JCPDS file 01-075-0449). However, the broad peaks, commonly observed when the powder has nanometric sizes, do not allow one to discard the presence of maghemite, because the latter has a structure similar to magnetite with comparable cell parameters.

7

However, Raman spectroscopy allows one to differentiate the iron oxide phases. The Raman spectra of nanoparticles (Fig. 1(b)) exhibit the characteristic bands of magnetite at 668 cm^{-1} assigned to the A_{1g} transition [26], confirming the absence of maghemite phase.
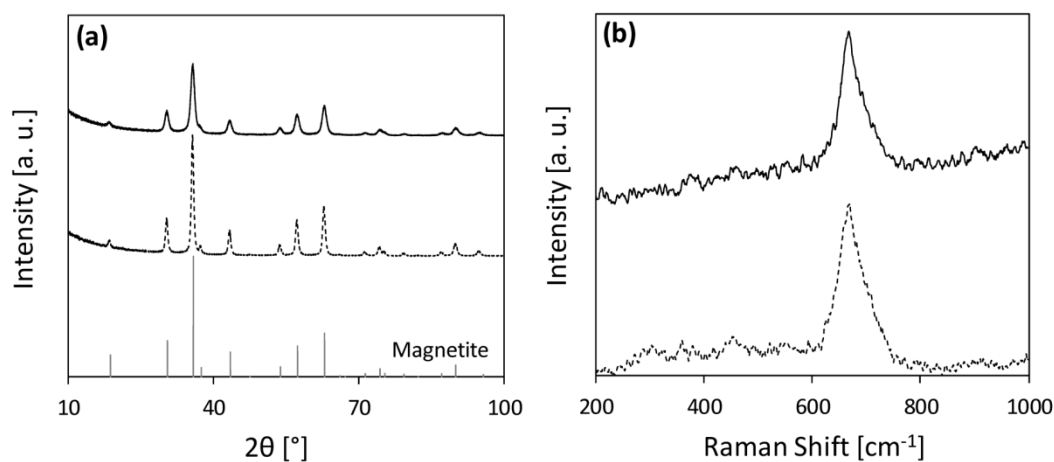

Fig. 1 XRD (a) and Raman (b) spectra of nanoparticle powders obtained respectively with 0.04 (dashed line) and 0.27 (solid line) mol/mol precursor-to-solvent ratio (chosen as representative samples)

The shape and the size of the primary particles were evaluated by TEM. Typical TEM micrographs, reported in Fig. 2, show that the synthesized powder has a nanostructured regular shape slightly changing as the precursor-to-solvent ratio increases. The dimensional analysis of TEM images indicates that the nanoparticle size is reduced with increasing the precursor concentration (from 19±4 to 10±2 nm).
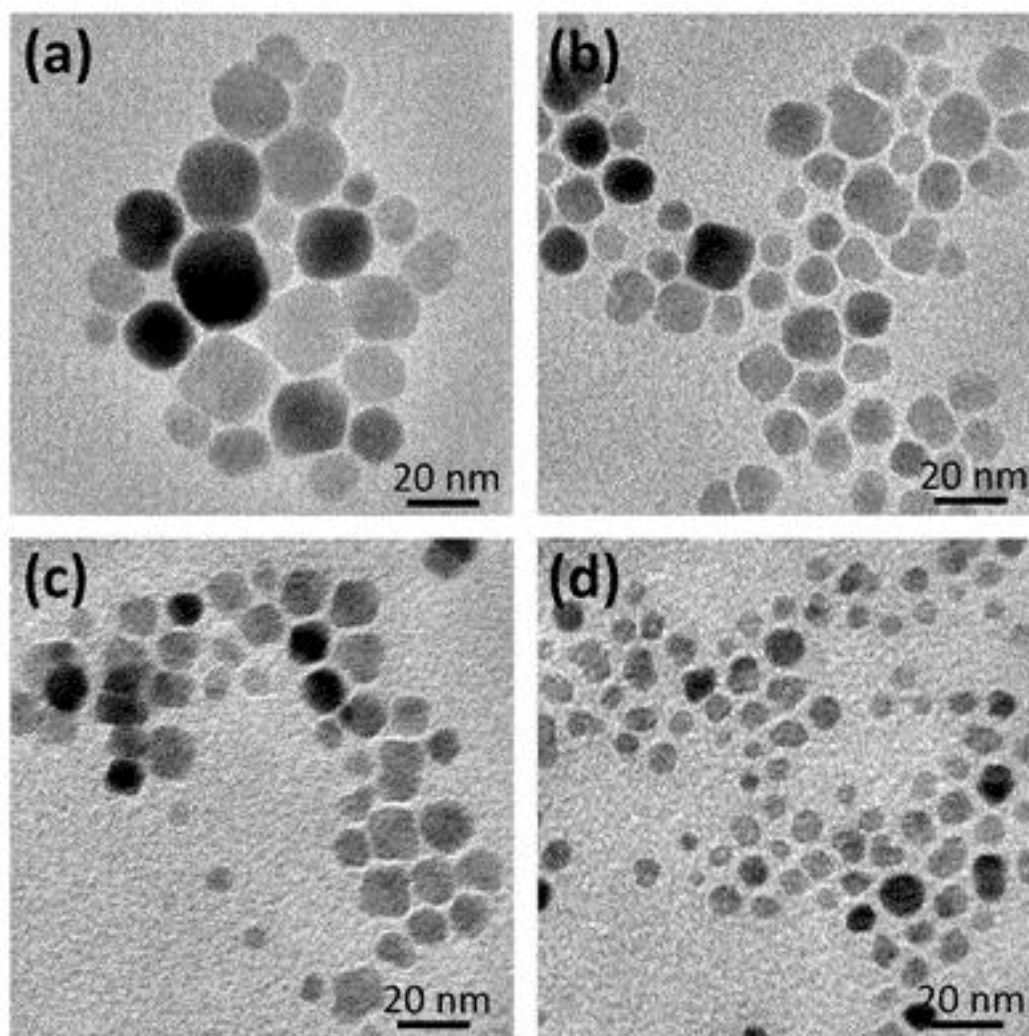
Fig. 2 TEM images of Fe_3O_4 powders, obtained at different precursor-to-solvent ratio: respectively 0.04 (a), 0.09 (b), 0.18 (c) and 0.27 (d) mol/mol.

As shown by FTIR spectra (Fig. 3), nanoparticles exhibit on their surface carboxylate groups, arising presumably from the oxidation of a hydroxyl group due to the reduction of Fe^{3+} to Fe^{2+}, and free alcoholic groups, presumably present in the same coordinating molecule. In fact, the bands in the range of 1600-1520 cm^{-1} and 1430-1320 cm^{-1} are assigned respectively to the asymmetrical and symmetrical vibrations of the carboxylate group [27], while the broad band at 3300 cm^{-1} is referred to the free hydroxyl group.
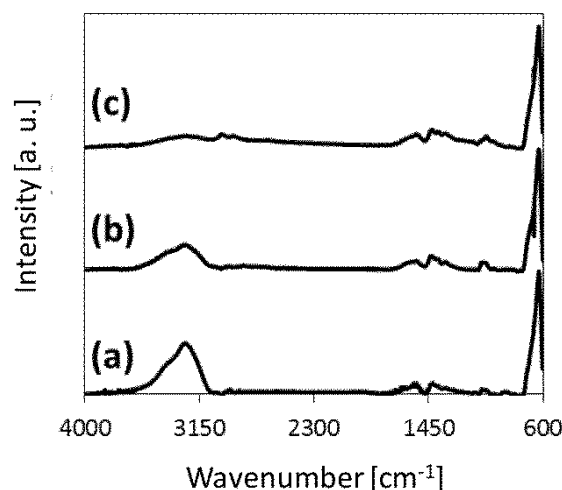
9

Fig. 3 FTIR spectra of the nanoparticle powders, obtained at different precursor-to-solvent ratio: respectively 0,04 (a), 0,18 (b) and 0,27 (c) mol/mol.

3.1 Epoxy-magnetite nanocomposite characterization

3.1.1 Structure, morphology and thermo-mechanical properties

The values of gel fraction, C_{gel}, are reported in Table 2. The C_{gel} values do not change significantly by increasing the amount of magnetite in the thermally-curable formulation and are even higher than the gel content of the unfilled resin, DGEBA-HD_0. The extractable/soluble fraction could be related to the molecules of DGEBA, HD and other by-products of the NHSG process which are not covalently linked to the three-dimensional network after curing reaction. In this respect, however, the analysis suggests that the reaction by-products do not limit the formation of a fully developed three-dimensional network. The presence of hydroxyl groups, both on the Fe_3O_4 nanoparticle surface (as underlined by FTIR) and due to the bi-functional alcoholic solvent (unreacted in the magnetite synthesis), can lead to a hydroxyl initiated polyetherification process. This mechanism, known as 'activated monomer' (AM) mechanism, is competitive with the conventional cationic 'active end chain' (ACE) mechanism and proceeds by nucleophilic attack of oxygen atom in hydroxyl end-group on carbon atom in protonated (activated) monomer molecule during the chain growth polymerization [28]. This hypothesis is supported by considering that the epoxy groups conversion, determined by FT-IR analysis, is very high and almost equal (98-99%, Table 2) for all composite materials, suggesting that it is possible to covalently incorporate both nanoparticles and their alcoholic suspending medium into the epoxy-based three-dimensional network.

Composite Code	C_{gel} [%]	C_{epoxy} [%]	T_g^{DSC} [°C]	T_g^{DMTA} [°C]	Experimental E'_{red}	Kerner E'_{red}
DGEBA-HD_0	90	98.7	29.9	34.2	1.00	1.000
DGEBA-HD_1	94.3	97.7	26.8	33.8	1.81	1.003
DGEBA-HD_2	94.1	98.1	32.7	33.7	3.81	1.006
DGEBA-HD_4	96.5	98.6	28.0	35.5	4.55	1.013
DGEBA-HD_6	94.5	98.5	29.1	34.7	5.78	1.020

Table 2 Gel content (C_{gel}), epoxy conversion (C_{epoxy}), glass transition temperature, obtained by DSC (T_g^{DSC}) and DMTA ($T_g^{\tan\delta}$) analysis, experimental and predicted reduced storage modulus (E'_{red}) of prepared composites.

STEM characterization of the composites permitted to evaluate the distribution and dispersion of magnetite nanoparticles in the matrix (Fig. 4). Homogeneous filler distribution was reached for all materials without using any coupling agents and/or lengthy and complex dispersion treatments. Even though the filler was well distributed, particle agglomerations in small magnetite domains were visible. This phenomenon was probably due to the common strong tendency of nanoparticles to aggregate, because of the high surface energy.

In all prepared samples, the dispersion tendency of the nanoparticles is relatively low, so that small island-like aggregates of magnetite nanoparticles are observed for all magnetite contents. However, quite surprisingly a better dispersion can be observed for the sample having the highest content of filler. This unexpected behavior could be tentatively ascribed, from a chemical point of view, to the formation of a nanoparticle surface with lower surface tension and a better compatibility with the surrounding organic matrix, which may minimize particle-particle interactions [23]. In fact, differences in chemical composition naturally arising from the variation in precursor-to-solvent ratio and the ensuing changes in the nanoparticle number and size concur in affecting the evolution of the network structure as a consequence of changes in thermodynamic factors and kinetic parameters during the network formation.
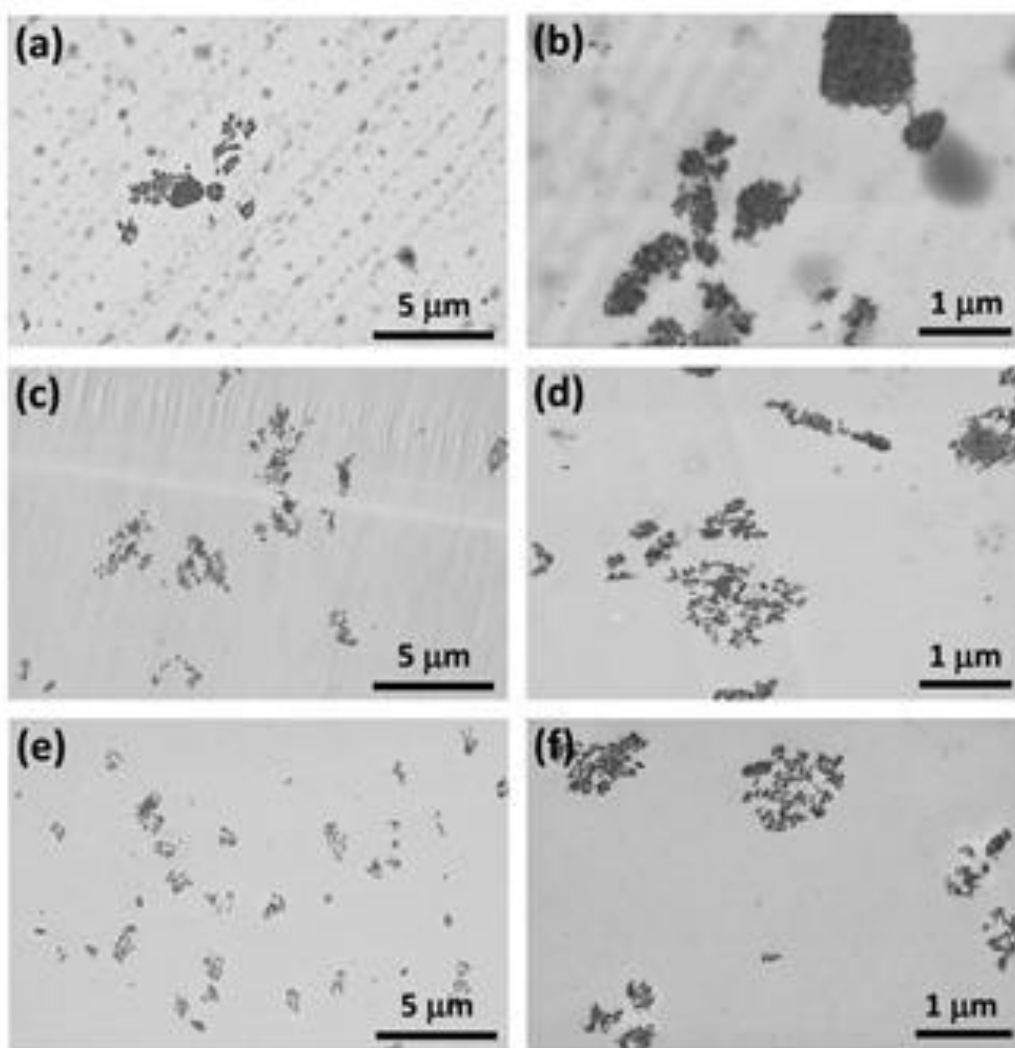
Fig. 4 STEM images of the magnetite nanocomposites at different magnification. The Fe_3O_4 content increases from top to bottom: DGEBA-HD_2 (a-b), DGEBA-HD_4 (c-d) and DGEBA-HD_6 (e-f).

DSC thermograms show that the glass transition temperature (T_g^{DSC}) is not significantly affected by increasing the magnetite content (Table 2). The same result was achieved by evaluating the glass transition temperature with the DMTA analysis (T_g^{DMTA}), expressed as maximum value of loss factor (Table 2). The fact that the T_g is not significantly affected by the presence of magnetite nanoparticles in the polymer could arise from the interplay between nanoparticles aggregates responsible of the reduced interphase volume and their specific interactions with the organic matrix. Moreover, the reduction in height and associated broadening of the loss factor peaks (Fig. 5a) imply an incrementally lower fraction of free polymeric chains with increasing filler fraction, due to nanoparticles-epoxy network interaction [29]. In particular, the observed reduction of the peak in the *tan δ* curves can be considered as an indirect indication of a specific filler-matrix interaction, as already

12

reported by Kim et al. [30] for epoxy nanocomposites containing silica nanoparticles functionalized with an interacting coupling agent.

The values of storage modulus E' obtained by DMTA analysis are reported in Fig. 5b. In the glassy state (that is, in the range 0-20°C) the storage moduli E' show only a slight dependence on the different amount of magnetite nanoparticles. A much stronger variation of E' is observed in the rubbery state and increases significantly by increasing the magnetite content.

Storage moduli were used to calculate the reduced storage modulus E'_{red}, i.e., the ratio between the moduli measured in nanocomposites and in the matrix, in the rubbery region. The experimental values of E'_{red} are reported in Table 2 as functions of magnetite volume fraction and compared with the predictions of the Kerner's model for composite materials [22,31]. The reported data indicate a relevant increase of E'_{red} with respect to the predictions of the generalized Kerner's equation. Considering that in the rubbery region the modulus is mainly governed by the cross-linking density of the network, the present results suggest that magnetite nanoparticle aggregates act not only as a rigid reinforcing filler but also as net-points, increasing the cross-linking density of the nanocomposites with respect to the epoxy matrix not containing the magnetic filler.
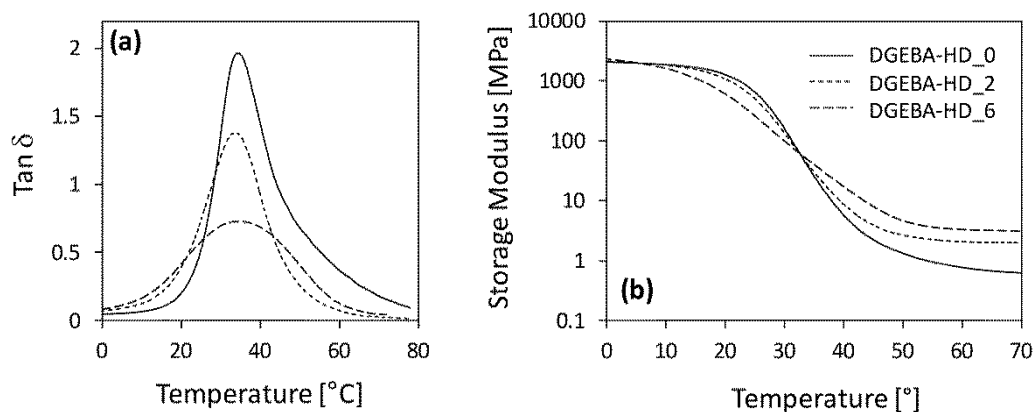

Fig. 5 Tanδ curves (a) and storage modulus (b) of DGEBA-HD_x samples.

3.1.1 Magnetic properties

Room-temperature hysteresis loops of all epoxy-magnetite nanocomposites measured in the range -70 kOe ≤ H ≤ +70 kOe are reported in Fig. 6. No significant coercive field is observed at T = 300 K: complete magnetic saturation is achieved in samples DGEBA-HD_1 and DGEBA-HD_2 whereas some unsaturating behavior is observed in both DGEBA-HD_4

and DGEBA-HD_6. The inset in Fig. 6 shows the magnetization at 70 kOe (M_S) as a function of nanoparticle concentration expressed by the phr parameter.
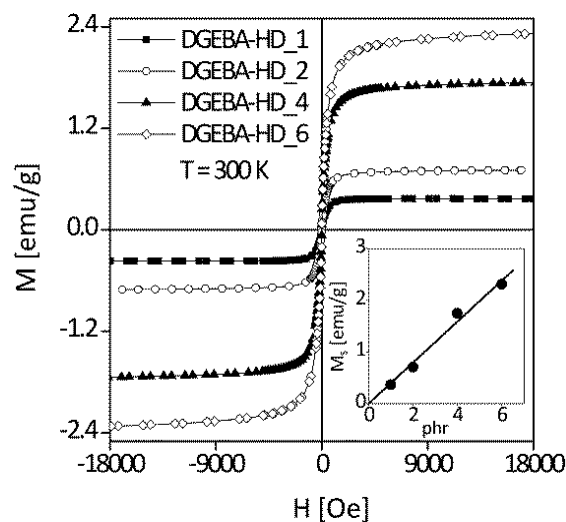

Fig. 6 Room-temperature hysteresis loops of all epoxy-magnetite nanocomposites. Inset: 70-kOe magnetization as a function of magnetite content (phr).

The temperature dependence of the coercive field H_c in the range 5-300 K is reported in Fig. 7 for all studied nanocomposites. The curves become steeper with increasing phr. The remanence-to saturation ratio (M_r/M_S) exhibits a closely similar temperature dependence (not reported).
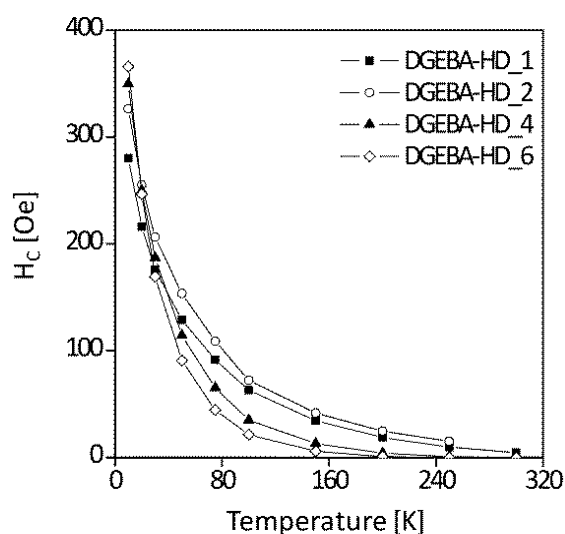

Fig. 7 Coercive field of all epoxy-magnetite nanocomposites as a function of temperature.

The initial magnetic susceptibility ($\chi_0 = (dM/dH)_H = 0$) is shown in Fig. 8 as a function of measurement temperature for all samples. The shape of the $\chi_0(T)$ curve gradually changes with increasing nanoparticle concentration: a monotonic, almost linear increase of χ_0 is found in DGEBA-HD_1 and DGEBA-HD_2, whereas a broad maximum of χ_0 at about 200 K is observed in DGEBA-HD_6 (DGEBA-HD_4 exhibits sort of an intermediate behavior).
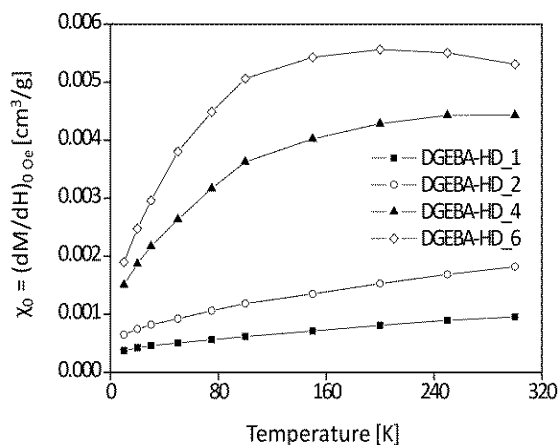

Fig. 8 Initial magnetic susceptibility as a function of temperature in all epoxy-magnetite nanocomposites.

The FC/ZFC curves taken under a field of 200 Oe and normalized to the starting value at T = 300 K are shown in Fig. 9. All nanocomposites display a rather flat, almost featureless FC curve and a ZFC curve, which does not exhibit any well-defined maximum at intermediate temperatures. In samples DGEBA-HD_1 and DGEBA-HD_2, both the FC and the ZFC curves increase with increasing temperature (with different slopes) and join at the merging temperature (T_{Mrg} = 285 K and 260 K, respectively), whereas in DGEBA-HD_4 and DGEBA-HD_6 the FC curves are characterized by a flat region at low T followed by a slight decrease; correspondingly, the steep slope of the ZFC curves decreases before merging with the corresponding FC curve. The merging temperatures are T_{Mrg} = 235 K in DGEBA-HD_4 and 200 K in DGEBA-HD_6. The behavior of T_{Mrg} as a function of nanoparticle concentration is shown in the inset.
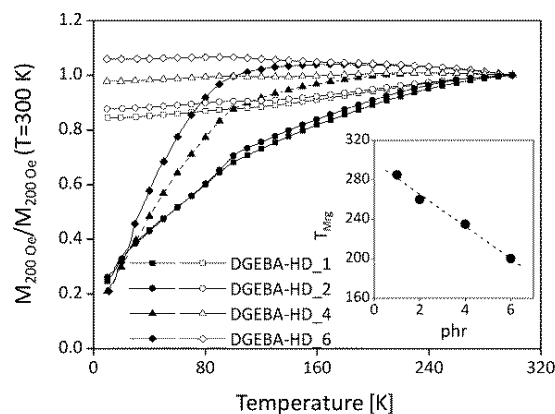
15

Fig. 9 Field-Cooled (FC; open symbols) and Zero-Field-Cooled (ZFC; full symbols) curves taken under a magnetic field of 200 Oe in all studied nanocomposites. For clarity, the curves were normalized to the value at T = 300 K. Inset: FC-ZFC curve merging temperature T_{Mrg} as a function of nanoparticle concentration.

The differential magnetic susceptibility at high fields ($\chi_{HF} = (dM/dH)_H = 15\ kOe$) is reported for all nanocomposites in Fig. 10. In samples DGEBA-HD_1 and DGEBA-HD_2, χ_{HF} monotonically decreases with increasing temperature and becomes vanishingly small above 100 K, in agreement with the data of Fig. 6 indicating complete saturation of the magnetization curves (*M(H)*) above 3 kOe at room temperature. In samples DGEBA-HD_4 and DGEBA-HD_6, a similar decrease of χ_{HF} up to about 100 K is observed; however, the slope of the *M(H)* curve never becomes zero and starts to increase again when T approaches room temperature, in such a way that a broad minimum of the $\chi_{HF}(T)$ curve is observed (the effect being more apparent in DGEBA-HD_6). The positive slope observed in the latter two samples reflects the unsaturating trend of the *M(H)* curves reported in Fig. 6.
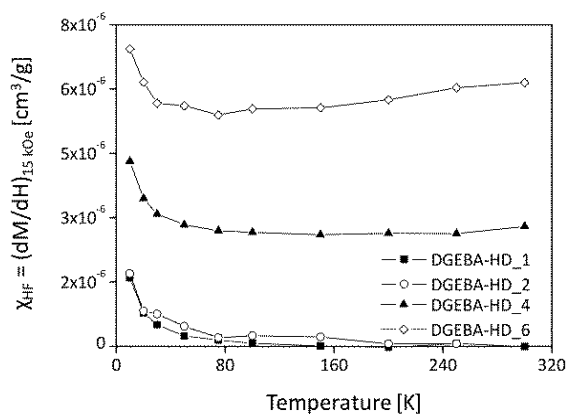

Fig. 10 High-field differential susceptibility (χ_{HF}) as a function of temperature in all epoxy-magnetite nanocomposites.

16

The temperature dependence of the initial susceptibility (Fig. 8) and the shape of the FC/ZFC curves (Fig. 9) indicate that the magnetic response of all studied nanocomposites is definitely not the one expected from a superparamagnetic (SP) material. In a pure/interacting superparamagnetic system (SP/ISP]) χ_0 is predicted to either behave as $1/T$ or as $1/(T + T^*)$ [32], T^* being the so-called dipolar temperature which measures the intensity of the dipolar interaction among moments in the ISP model [33]. In all studied materials, instead, the initial susceptibility follows a quite opposite behavior, being observed to increase with increasing T: in samples DGEBA-HD_1/2/4 such an increase is monotonic, while in DGEBA-HD_6 χ_0 grows at low temperature and weakly decreases above 200 K.

The FC/ZFC curves of DGEBA-HD_1 and DGEBA-HD_2 are quite similar and indicate that both nanocomposites behave as strongly correlated or ferromagnetic materials in agreement with the results of Fig. 8: in fact, in a ferromagnetic material the initial susceptibility usually increases with increasing temperature [34]. The FC/ZFC curves measured in samples DGEBA-HD_4 and DGEBA-HD_6 partly retain similar features, indicating that a strong magnetic correlation among nanoparticles exists also in these nanocomposites; however, a plateau is observed below 100 K in the FC curves; in the same region, the corresponding ZFC curves exhibit a much steeper increase with increasing T. These features are typical of a frozen collective disordered state of magnetic moments, such a super-spin glass state [35].

The merging temperatures of FC/ZFC curves steadily increase towards 300 K with decreasing phr. It should be noted that in a ferromagnetic material the merging temperature is coincident with the starting temperature of the measurement cycle (i.e., 300 K in the present case): this result supports the previous conclusions, indicating that all samples contain a ferromagnetic phase which becomes dominant with decreasing phr.

Fig. 11 ((a) and (c)) definitely shows that the scaling law expected in a genuine SP system is never fulfilled (not even near room temperature) in samples DGEBA-HD_1 and DGEBA-HD_6 (the remaining two samples exhibiting the very same behavior, not shown here); on the other hand, the inadequacy of the ISP model is indicated by the rather bad agreement of the experimental data with the predicted scaling law [33] (Fig. 11 (b) and (d)). As known [36], the ISP model can be applied when the interaction among nanoparticles is sufficiently weak to be approximated by a mean-field term; Fig. 11 indicates that magnetic interactions are too strong in all the considered materials to be accounted for by a mean-field theory, even if a better agreement with the ISP model scaling prediction is found in DGEBA-HD_6.
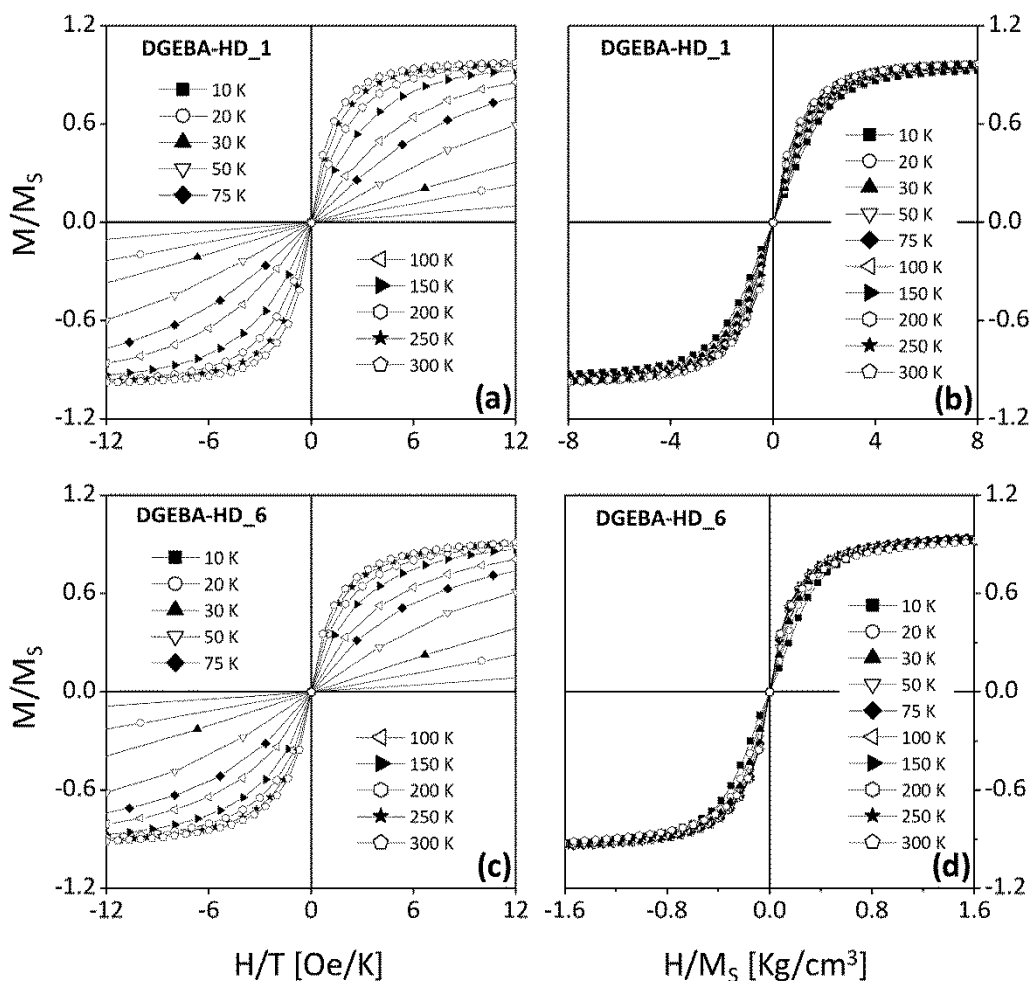
Fig. 11 Normalized anhysteretic magnetization curves extracted from measurements at temperatures between 10 and 300 K and plotted as functions of H/T (a) and (c)) and of H/M_s ((b) and (d)) in DGEBA-HD_1 (top row) and DGEBA-HD_6 (bottom row) nanocomposites.

The common feature of the high-field susceptibility vs. temperature curves (Fig. 10) is the decrease of χ_{HF} with increasing T from 10 K to about 100 K, connected with a distinctly unsaturating behavior of the isothermal *M(H)* curves; this result indicates that a frozen, disordered magnetic phase exists in all examined samples at low temperatures. Above 100 K, both samples DGEBA-HD_1 and DGEBA-HD_2 behave as genuine ferromagnetic materials displaying ordinary magnetic saturation at high fields ($\chi_{HF} \rightarrow 0$); this result supports the interpretation stemming from Fig. 8 and 9. On the contrary, in both samples DGEBA-HD_4 and DGEBA-HD_6 the high-field susceptibility does not become zero above 100 K, indicating that a magnetically disordered, weakly saturating phase exists at all temperatures; in sample DGEBA-HD_6, χ_{HF} begins to increase with increasing T above about 150 K (a similar effect, although less definite, can be observed in DGEBA-HD_4 also).

As a matter of fact, in both SP and ISP systems, the high-field susceptibility, proportional to the derivative of the Langevin function with respect to the magnetic field, is expected to behave as T or (T+T*), respectively. We therefore conclude that in DGEBA-HD_6 (and possibly in DGEBA-HD_4) a fraction of magnetic moments begins to show a SP/ISP response at high temperatures, in agreement with the behavior of χ_0 in the same material (Fig. 8).

A comparison of these results with the STEM images (Fig. 4.) allows one to draw a microscopic picture of the magnetic state in these materials based on the different degree and nature of morphologic and magnetic order in the aggregates of nanoparticles, which are observed to exist in all studied materials.

As graphically represented in Fig. 12 (not to scale), inside each aggregate of nanoparticles the magnetic nanoparticles are expected to be strongly coupled, magnetic contact interactions playing a dominating role; in fact, the magnetic exchange length [37] is higher than the typical nanoparticle size, resulting in a ferromagnetic arrangement of the individual magnetic moments in the core of each aggregate; such an ordered state is rather robust, being preserved in the whole temperature interval from 10 to 300 K. However, a disordered state of nanoparticle moments is expected to be present at the surface of each aggregate; at very low temperatures, the moments at the surface of each aggregate undergo collective freezing, resulting in the super-spin-glass response evidenced by Figs. 12 (left panels): such a response is superimposed to the ferromagnetic signal stemming from the core of the aggregate.

When the temperature is increased, the collective disordered state at the surface of an aggregate gradually unfreezes. However, when the single nanoparticles are larger and the aggregates are particularly dense and regular, as in the sample DGEBA-HD_2 (Fig. 4), the magnetic moments at the surface of the aggregate feel the ordering effect from the ferromagnetic core and eventually align to the common direction of the magnetization in the entire aggregate. As a consequence, the system as a whole behaves ferromagnetically even at high temperatures (T > 100 K), each aggregate responding as an individual ferromagnetic entity to the applied field; the magnetic interaction among distant aggregates is deemed negligible. In samples where the single nanoparticles are smaller and the aggregates are less dense and characterized by a sort of branched structure, as in samples DGEBA-HD_4 and DGEBA-HD_6, the unfreezing moments at the surface are less affected by the ordering effect of the core and begin to act as nearly-free above about 100 K, mimicking the behavior of a SP/ISP material.
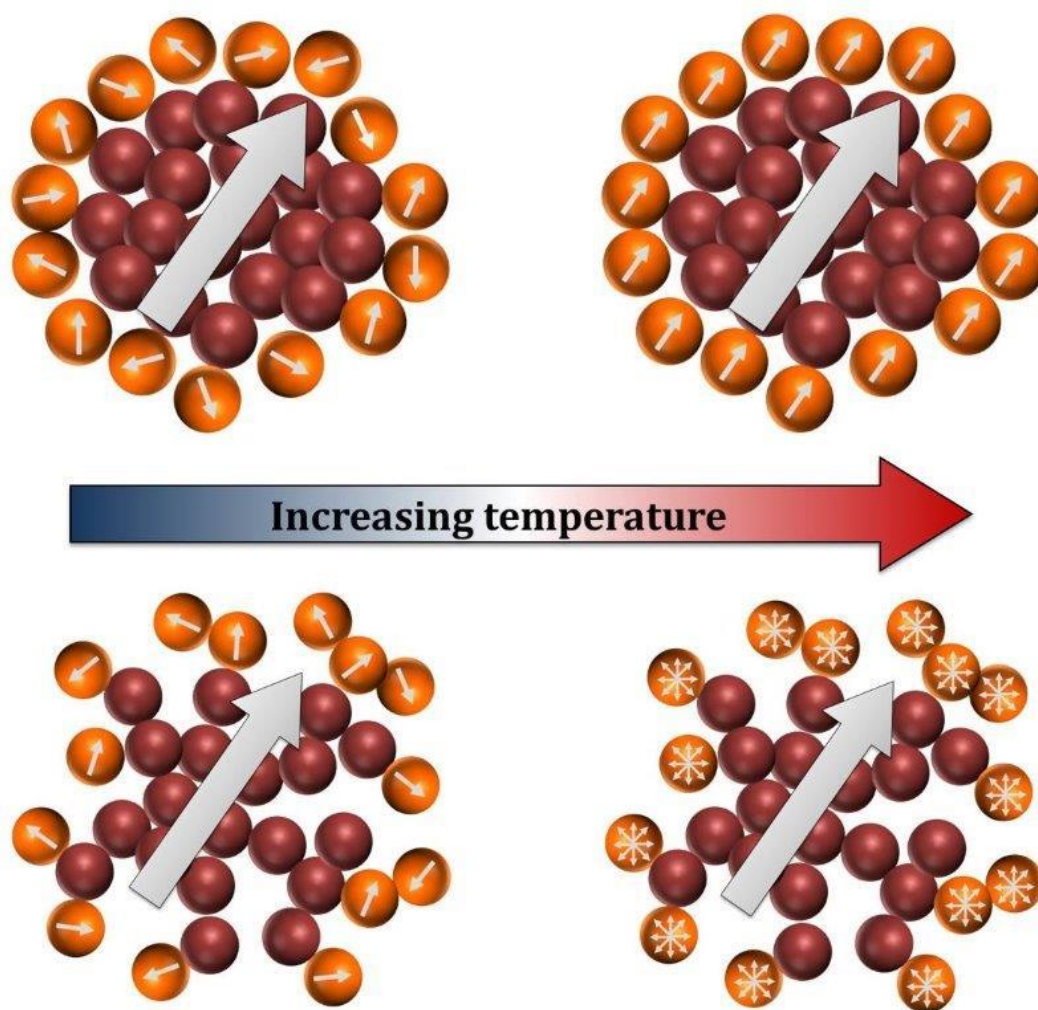
Fig. 12 Schematic representation of the degree of magnetic order in nanoparticle aggregates. The upper panel depicts the behaviour of samples DGEBA-HD_1-2; the lower panel is more appropriate to describe samples DGEBA-HD_4-6. The multiple arrows in the lower right panel indicate a SP/ISP behavior. All panels illustrate the magnetic arrangements expected under a moderate magnetic field (H $\cong$ 1000 Oe) wiping out all magnetic inhomogeneities (e.g., magnetic domains, domain walls) in the ferromagnetic cores.

4. Conclusions

Suspensions of magnetite nanoparticles in HD were synthesized by means of NHSG process and mixed with DGEBA monomers and subsequently crosslinked through a thermally activated cationic polymerization to obtain a nano-filled epoxy resin. HD molecules not reacted during the nanoparticle synthesis were covalently linked to the epoxy network as reactive co-monomer, suggesting that the chain-growth mechanism functional to produce the epoxy polymer was able to involve other suitable reactive species in the ring-opening polymerization during the reaction propagation.

The synthesis of nanometer-sized magnetite and the subsequent polymerization of the suspending medium resulted in a very strong filler–matrix interaction with a significant improvement in the cross-linking density due to the magnetite contribution. In fact, the enhancement of storage modulus in the rubbery region with increasing filler content support the hypothesis that the particles are able to act not only as a rigid filler but also as cross-linking densifier, leading to an increase in cross-linking density.

All studied nanocomposites exhibit a particularly complex magnetic behavior related to the coexistence of different magnetic phases whose effect and relative magnitude are changing as functions of measurement temperature. The saturation magnetization of the four nanocomposites is linearly correlated with the phr of the magnetic filler. Both STEM images and FC/ZFC curves indicate that all materials contain magnetic aggregates comprised of many individual nanoparticles; at low temperatures, all aggregates display a ferromagnetic-like response; however, in samples DGEBA-HD_4 and DGEBA-HD_6 the strength of interaction is lower, so that some nanoparticles (in our model, those situated at the boundaries of the aggregates) begin to unblock by effect of increasing temperature, behaving as basically superparamagnetic. Instead, in the other two samples the interparticle interaction is so strong that a ferromagnetic-like response is measured up to room temperature.

References

[1] P. Judeinstein, C. Sanchez, Hybrid organic–inorganic materials: a land of multidisciplinarity, *J. Mater. Chem.,* 6, (1996) 511-525.

[2] D. Y. Godovski, Electron behavior and magnetic properties of polymer nanocomposites, in: Y. K. Godovsky, V. P. Privalko (Eds.), Thermal and Electrical Conductivity of Polymer Materials, Springer, Berlin, Heidelberg, 1995, pp. 79-122.

[3] P. Kim, N. M. Doss, J. P. Tillotson, P. J. Hotchkiss, M.-J. Pan, S. R. Marder, J. Li, J. P. Calame, J. W. Perry, High energy density nanocomposites based on surface-modified $BaTiO_3$ and a ferroelectric polymer, *ACS Nano, 3*, (2009) 2581-2592.

[4] J. Zhu, S. Wei, J. Ryu, L. Sun, Z. Luo, Z. Guo, Magnetic Epoxy Resin Nanocomposites Reinforced with Core−Shell Structured Fe@FeO Nanoparticles: Fabrication and Property Analysis, *ACS Appl. Mater. Interfaces, 2*, (2010) 2100-2107.

[5] Z. Guo, S. Park, H. T. Hahn, S. Wei, M. Moldovan, A. B. Karki, D. P. Young, Magnetic and electromagnetic evaluation of the magnetic nanoparticle filled polyurethane nanocompositesm *J. Appl. Phys., 101*, (2007) 09M511.

[6] A. Alfadhel, B. Li, J. Kosel, Magnetic Polymer Nanocomposites for Sensing Applications, *IEEE SENSORS 2014* Proceedings, (2014) 2066-2069.

[7] P. Allia, M. Sangermano, A. Chiolerio, Magnetic Properties of Polymer Nanocomposites, in: A. Dasari and J. Njuguna (Eds.) Functional and Physical Properties of Polymer Nanocomposites, John Wiley & Sons, Ltd, 2016, pp. 119-138.

[8] P. Allia, G. Barrera, P. Tiberto, T. Nardi, Y. Leterrier, M. Sangermano, Fe_3O_4 nanoparticles and nanocomposites with potential application in biomedicine and in communication technologies: Nanoparticle aggregation, interaction, and effective magnetic anisotropy, J. Appl. Phys., *116*, (2014) 113903.

[9] N. Florini, G. Barrera, P. Tiberto, P. Allia, F. Bondioli, Nonaqueous sol–gel synthesis of magnetic iron oxides nanocrystals, J. Am. Ceram. Soc., *96*, (2013) 3169-3175.

[10] H.-J. Chen, P.-C. Jian, J.-H. Chen, L. Wang, W.-Y. Chiu, Nanosized-hybrid colloids of poly(acrylic acid)/titania prepared via in situ sol–gel reaction, Ceram. Int., *33*, (2007) 643-653.

[11] J. Jordan, K. I. Jacob, R. Tannenbaum, M. A. Sharaf, I. Jasiuk, Experimental trends in polymer nanocomposites—a review, Mater. Sci. Eng.: A, *393*, (2005) 1-11.

[12] M. Tamborra, M. Striccoli, R. Comparelli, M. L. Curri, A. Petrella, A. Agostiano, Optical properties of hybrid composites based on highly luminescent CdS nanocrystals in polymer, Nanotechnology, 15, (2004) S240-S244.

[13] C. Sciancalepore, T. Cassano, M. L. Curri, D. Mecerreyes, A. Valentini, A. Agostiano, R. Tommasi, M. Striccoli, TiO_2 nanorods/PMMA copolymer-based nanocomposites: highly homogeneous linear and nonlinear optical material, Nanotechnology, *19*, (2008) 205705.

[14] C. Sanchez, B. Julian, P. Belleville, M. Popall, Applications of hybrid organic–inorganic nanocomposites, J. Mater. Chem., *15*, (2005) 3559-3592.

[15] I. Bilecka, M. Niederberger, New developments in the nonaqueous and/or non-hydrolytic sol–gel synthesis of inorganic nanoparticles, Electrochim. Acta, *55*, (2010) 7717-7725.

[16] N. Pinna, G. Neri, M. Antonietti, M. Niederberger, Nonaqueous Synthesis of Nanocrystalline Semiconducting Metal Oxides for Gas Sensing, Angew. Chem., Int. Ed., *43*, (2004) 4345-4349.

[17] C. Sciancalepore, R. Rosa, G. Barrera, P. Tiberto, P. Allia, F. Bondioli, Microwave-assisted nonaqueous sol–gel synthesis of highly crystalline magnetite nanocrystals, Mater. Chem. Phys., *148*, (2014) 117-124.

[18] P. H. Mutin, A. Vioux, Nonhydrolytic Processing of Oxide-Based Materials: Simple Routes to Control Homogeneity, Morphology, and Nanostructure, Chem. Mater., *21*, (2009) 582-596.

[19] C. Sciancalepore, F. Bondioli, M. Messori, G. Barrera, P. Tiberto, P. Allia, Epoxy nanocomposites functionalized with in situ generated magnetite nanocrystals: Microstructure, magnetic properties, interaction among magnetic particles, Polymer, *59*, (2015) 278-289.

[20] D. Morselli, F. Bondioli, M. Sangermano, M. Messori, Epoxy networks reinforced with TiO_2 generated by nonhydrolytic sol–gel process: A comparison between in situ and ex situ syntheses to obtain filled polymers, Polym. Eng. Sci., 55, (2015) 1689-1697.

[21] D. Morselli, F. Bondioli, M. Sangermano, M. Messori, Photo-cured epoxy networks reinforced with TiO_2 in-situ generated by means of non-hydrolytic sol–gel process, Polymer, 53, (2012) 283-290.

[22] D. Morselli, F. Bondioli, M. Sangermano, I. Roppolo, M. Messori, Epoxy resins reinforced with TiO2 generated by nonhydrolytic sol–gel process, J. Appl. Polym. Sci., 131, (2014) 40470.

[23] C. Sciancalepore, F. Bondioli, M. Messori, Non-hydrolytic sol–gel synthesis and reactive suspension method: an innovative approach to obtain magnetite–epoxy nanocomposite, J. Sol-Gel Sci. Technol., (2016) 1-15.

[24] L. E. Nielsen, Generalized equation for the elastic moduli of composite materials, *J. Appl. Phys.,* 41, (1970) 4626-4627.

[25] R. F. Landel and L. E. Nielsen, *Mechanical Properties of Polymers and Composites, Second Edition*, CRC press, 1993.

[26] T. J. Daou, G. Pourroy, S. Bégin-Colin, J. M. Grenèche, C. Ulhaq-Bouillet, P. Legaré, P. Bernhardt, C. Leuvrey, G. Rogez, Hydrothermal Synthesis of Monodisperse Magnetite Nanoparticles, Chem. Mater., 18, (2006) 4399-4404.

[27] Y. Lu, J. D. Miller, Carboxyl Stretching Vibrations of Spontaneously Adsorbed and LB-Transferred Calcium Carboxylates as Determined by FTIR Internal Reflection Spectroscopy, J. Colloid Interface Sci., 256 (2002) 41-52.

[28] P. Chabanne, L. Tighzert, J.-P. Pascault, Monoepoxy polymerization initiated by BF_3-amine complexes in bulk. II. Influence of water and by-products on polymer formation, J. Appl. Polym. Sci., 53, (1994) 769-785.

[29] A. Strachota, I. Kroutilová, J. Kovářová, L. Matějka, Epoxy Networks Reinforced with Polyhedral Oligomeric Silsesquioxanes (POSS). Thermomechanical Properties Macromolecules, 37, (2004) 9457-9464.

[30] S. Kang, S. I. Hong, C. R. Choe, M. Park, S. Rim and J. Kim, Preparation and characterization of epoxy composites filled with functionalized nanosilica particles obtained via sol–gel process, Polymer, 42, (2001) 879-887.

[31] E. H. Kerner, The Elastic and Thermo-elastic Properties of Composite Media, Proceedings of the Physical Society. Section B, 69, (1956) 808-813.

[32] M. Knobel, W. C. Nunes, L. M. Socolovsky, E. De Biasi, J. M. Vargas, J. C. Denardin, Superparamagnetism and other magnetic features in granular materials: a review on ideal and real systems, J. Nanosci. Nanotechnol., 8, (2008) 2836-2857.

[33] P. Allia, P. Tiberto, Dynamic effects of dipolar interactions on the magnetic behavior of magnetite nanoparticles, J. Nanopart. Res., 13, (2011), 7277-7293.

[34] S. Chikazumi, *Physics of Ferromagnetism*, OUP Oxford, 2009.

[35] D. Fiorani, D. Peddis, Understanding dynamics of interacting magnetic nanoparticles: from the weak interaction regime to the collective superspin glass state, J. Phys.: Conf. Ser., 521, (2014) 012006.

[36] P. Allia, Fe-oxide Nanoparticles: a natural playground for testing the ISP model, J. Phys.: Conf. Ser., 521, (2014) 012008.

[37] J. M. D. Coey, *Magnetism and Magnetic Materials*, Cambridge University Press, 2010.

Magnetite-epoxy nanocomposites obtained by the reactive suspension method: microstructural, thermo-mechanical and magnetic properties

G. Barrera,[a] C. Sciancalepore,[b] M. Messori,[c] P. Allia[*,d] P. Tiberto[a] and F. Bondioli[b,e]

Graphical abstract
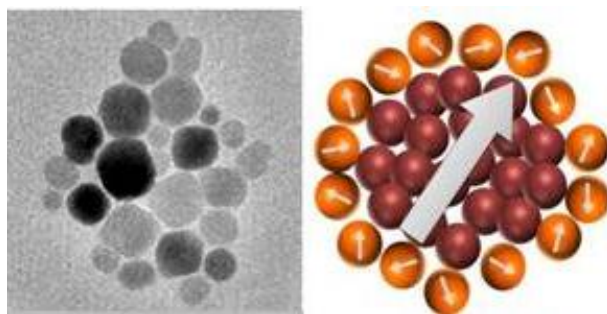
Highlights

- A single organic agent is exploited in the whole preparation process

- Magnetic nanoparticles form aggregates in polymeric nanocomposites

- Size and nature of magnetic aggregates depend on synthesis parameters